

Low-velocity impact of composites plates using the Radial Point Interpolation Method

A. Djeukou¹ and O. von Estorff²

Abstract: The paper deals with the response of rectangular composite plates to low-velocity impact. A third-order shear deformation theory as well as the Newmark integration are used to determine the contact force history analytically. The interaction between the impactor and the plate is modeled with the help of a two degrees-of-freedom system, consisting of springs and masses. The Choi's linearized Hertzian contact model is used to determine the contact force. The maximum impact force is employed for a static damage analysis of the composite plate by means of the radial point interpolation method, while the Tsai-Wu failure criterion is applied for the modeling of damage. Several examples are investigated and the results compared to those available in the literature.

Keywords: low-velocity impact, composites, delamination, meshless methods.

1 Introduction

Composite materials have become very essential constituents within the aeronautical field. They are characterized, among other things, by their low density and load-oriented design capability. These properties cleverly used result in big weight savings compared to isotropic metallic structures.

Driven by the intention to save weight, many metallic aircraft components are being replaced by comparable composites structures that bring out some important new issues in the design. One of these issues is the impact behavior of the structure, for example of the flaps due to runway debris. Due to the lack of exact knowledge of the composite behavior in the case of impacts, conservative approaches, such as assuming a hole at impact location, are used during the design. A good understanding of the behavior of composites might lead to a smarter setup, a more adequate construction, and consequently to a considerable weight reduction.

¹ c/o Airbus Deutschland GmbH, Bremen, Germany, djeumel@hotmail.com.

² Institute of Modeling and Computation, Hamburg University of Technology, Hamburg, Germany.

Extensive test campaigns have been performed by researchers developing contact law formulations [Sun (1977), Yang and Sun (1981), Willis (1966)]. Analytical methods have then been developed for the contact force history determination [Choi and Lim (2004), Khalili, Shokuhfar, and Ashenai Ghasemi (2007), Abrate (2001), Cantwell and Morton (1991)], and it was found that for a detailed study of the layer behavior, discretization methods, such as the finite element method (FEM), are required.

However, the FEM exhibits the typical shortcomings of all numerical methods based on meshes or elements which are connected by nodes: High element deformation ratios are not allowed. Consequently, in some analyses meshing and re-meshing are necessary, burdensome, and often lead to difficulties when dealing with impact problems.

To overcome these drawbacks, a new class of methodologies, namely so called "meshfree methods" has been developed and achieved remarkable progress over the past few years [Chen, Liu, and Lim (2003), Krysl and Belytschko (1995), Liu (2002), Liu and Gu (2005), Sladek, Sladek, Zhang, Sulek, and Starek (2007), Shan, Shu, and Lu (2008), Wen-Hwa, Cheng-Te, and Ming-Hsiao (2009)]. Hagihara applied the element free Galerkin method (EFG) for solving elastic-plastic problems Hagihara, Tsunori, Ikeda, and Miyazaki (2007). An example of the application of the meshless local Petrov-Galerkin method (MLPG) in the deformation analysis of shells can be seen in Jarak, Sori, and Hoster (2007).

All meshless methods have in common that they do not require an element discretization of the problem domain. The approximation functions are constructed entirely in terms of a set of nodes, and no element or connectivity of the nodes is needed. In view of this, meshfree methods have a very good potential to become a powerful new generation of numerical technologies in the future. Among these formulations, the radial point interpolation method (RPIM), suggested by Liu [Liu and Gu (2001), Liu (2002), and Liu and Gu (2005)] turned out to be a stable mesh-free method that allows direct enforcement of essential boundary conditions due to its Kronecker delta function properties. For this reason, it has been chosen for the investigations in this work.

In the present study, the contact force history is determined using the Choi's linearized contact law [Choi and Lim (2004)] and Newmark integration. The third order shear deformation theory of Reddy (TSDT) [Reddy (1997)] is used for modeling the composite plate. The problem domain is discretized by a set of nodes and the constitutive equations are solved by means of the RPIM. A two-dimensional Tsai-Wu failure criterion is used to predict the layer failure. Finally, the results are compared to computations and to measurements found in the literature.

2 Dynamic impact response of the plate

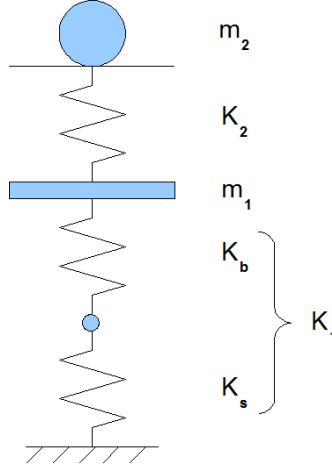


Figure 1: Spring masses model

In the present analysis, the two degrees of freedom spring-mass model [Choi and Lim (2004)], given in Fig. 1, is utilized to determine the contact force of the impact. Its transient behavior is described by the equations of motion Khalili, Shokuhfar, and Ashenai Ghasemi (2007),

$$\begin{aligned} m_2 \ddot{z}_2 + F &= 0 \\ m_1 \ddot{z}_1 + K_1 z_2 - F &= 0, \end{aligned} \quad (1)$$

where F is the contact force, m_1 and m_2 represent the mass of the composite plate and the impactor, respectively, z_1 and z_2 are the relative displacements of the composite plate and the impactor masses. K_1 is the bending-shear stiffness of the composite plate defined as

$$\begin{aligned} K_1 &= \left(\frac{1}{K_b} + \frac{1}{K_s} \right)^{-1} \\ K_b &= \frac{4\pi E_r t^3}{3(3+\nu_r)(1-\nu_r)a^2} \\ K_s &= \frac{4\pi G_{zr} t}{3} \left(\frac{E_r}{E_r - 4\nu_r G_{zr}} \right) \left[\frac{1}{\frac{4}{3} + \log\left(\frac{a}{ac}\right)} \right] \cdot \\ a &= \frac{w}{2} \\ w &= \lambda b \end{aligned} \quad (2)$$

K_b is the plate bending stiffness and K_s the plate shear stiffness. t denotes the plate thickness, E_r is the Young's modulus of the plate in radial direction, G_{zr} is the

shear modulus in the radial and through-the-thickness plane, assumed to be equals to $E_r/2(1 + \nu_r)$, ν_r is the Poisson's ratio, here assumed to be 0.3. a is the impact model radius ($w/2$) according to Fig. 2, a_c is the radius of the contact area assumed to be $t/2$. λ depends on the type of boundary conditions. It needs to be determined by comparisons with test results. Investigations done within this work have shown that λ should be equals to 1.0 in the case of simply supported boundary conditions, and 0.7 in the case of clamped edges.

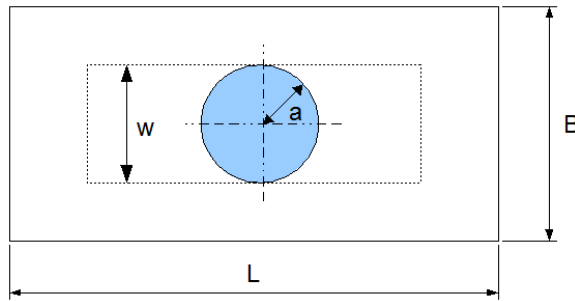


Figure 2: Plate impact model

Hence, using Choi's linearized model [Choi and Lim (2004)] instead of the nonlinear Hertzian contact law, the contact force can be obtained as

$$\begin{aligned} F &= K_2 (z_2 - z_1) \\ K_2 &= F_m^{1/3} K_c^{2/3} \\ K_c &= \frac{4}{3} \frac{R^{1/2}}{((1-\nu^2)/E) + (1/E_{22})} \end{aligned} \quad (3)$$

In the equations above, K_2 represents the linearized contact coefficient in Choi's contact law, F_m is the maximum predicted contact force, and K_c is the contact stiffness in the modified Hertzian contact law. R denotes the curvature radius, ν is the Poisson's ratio and E is the elastic modulus of the isotropic impactor. Since the plate is not isotropic, it must be mentioned that the parameter E_{22} is the transverse elastic modulus of the top lamina of the structure.

Considering the model defined in Fig. 1 and replacing F in Eq. 1 by the term given in Choi's differential equations, one obtains, after rearrangements, the form:

$$\begin{aligned} m_1 \ddot{z}_1 + (K_1 + K_2) z_1 - K_2 z_2 &= 0 \\ m_2 \ddot{z}_2 - K_2 z_1 + K_2 z_2 &= 0. \end{aligned} \quad (4)$$

This system may be solved with the Newmark integration method. The maximum contact force from the force history will be used later on for a static damage analysis.

2.1 Radial point interpolation method (RPIM)

Consider a field function $u(\mathbf{x})$ which is defined in the problem domain Ω and discretized by a set of field nodes. Then the RPIM interpolation can be written as

$$u(x) = \sum_{i=1}^n R_i(\mathbf{x})a_i + \sum_{j=1}^m p_j(\mathbf{x})b_j = \mathbf{R}^T(\mathbf{x})\mathbf{a} + \mathbf{p}^T(\mathbf{x})\mathbf{b}, \quad (5)$$

where $R_i(\mathbf{x})$ is a radial basis function (RBF), n is the number of RBFs, $p_i(\mathbf{x})$ is a monomial in the space coordinate $\mathbf{x}^T = [x, y]$, and m is the number of polynomial basis functions. When $m = 0$, only RBFs are used. Otherwise, the RBF is augmented with m polynomial basis functions. The coefficients a_i and b_j are constants to be determined yet.

In the radial basis function $R_i(\mathbf{x})$, the only variable is the distance between the point of interest \mathbf{x} and a node at \mathbf{x}_i , i.e. for 2-D problems one obtains

$$r = \sqrt{(x - x_i)^2 + (y - y_i)^2}. \quad (6)$$

There exist a number of different types of radial basis functions. Four often used RBFs, namely the multi-quadrics (MQ) function, the Gaussian (Exp) function, the thin plate spline (TPS) function, and the Logarithmic radial basis function, are listed in Tab. 1. In utilizing RBFs, several shape parameters need to be determined in order to obtain a good performance. In general, for given types of problems these parameters can be determined by numerical examinations. For example in the MQ-RBF, there are two shape parameters, α_c and q , to be determined. In previous work by the authors [Djeukou and von Estorff (2009)], it has been shown, that $q = \pm 0.5$ and $\alpha_c d_c = 12$ lead to proper results for composite plate analyses.

Table 1: Typical radial basis functions with dimensionless shape parameters

	Name	Expression	Shape parameters
1	Multi-quadrics (MQ)	$R_i(x, y) = (r_i^2 + (\alpha_c d_c)^2)^q$	$\alpha_c \geq 0, q$
2	Gaussian (EXP)	$R_i(x, y) = \exp \left[-\alpha_c \left(\frac{r_i}{d_c} \right)^2 \right]$	α_c
3	Thin Plate Spline (TPS)	$R_i(x, y) = r_i^\eta$	η
4	Logarithmic	$R_i(x, y) = r_i^\eta \log r_i$	η

In order to determine a_i and b_j in Eq. 5, a support domain is formed for the point of interest at \mathbf{x} , and n field nodes are included in the support domain. Coefficients a_i and b_j in Eq. 5 can be determined by enforcing Eq. 5 to be satisfied at these n

nodes surrounding the point of interest at \mathbf{x} . This leads to n linear equations, one for each node. The matrix form of these equations can be expressed as

$$\mathbf{U}_s = \mathbf{R}_0 \mathbf{a} + \mathbf{P}_m \mathbf{b}. \quad (7)$$

When the vector of the function values \mathbf{U}_s is defined by

$$\mathbf{U}_s = \{u_1 \ u_2 \ \dots \ u_n\}^T, \quad (8)$$

\mathbf{R}_0 is the moment matrix of the RBFs given in the form

$$\mathbf{R}_0 = \begin{bmatrix} R_1(r_1) & R_2(r_1) & \dots & R_n(r_1) \\ R_1(r_2) & R_2(r_2) & \dots & R_n(r_2) \\ \dots & \dots & \dots & \dots \\ R_1(r_n) & R_2(r_n) & \dots & R_n(r_n) \end{bmatrix}_{(n \times n)}, \quad (9)$$

and the polynomial moment matrix is given by

$$\mathbf{P}_m^T = \begin{bmatrix} 1 & 1 & \dots & 1 \\ x_1 & x_2 & \dots & x_n \\ y_1 & y_2 & \dots & y_n \\ \vdots & \vdots & \ddots & \vdots \\ p_m(\mathbf{x}_1) & p_m(\mathbf{x}_2) & \dots & p_m(\mathbf{x}_n) \end{bmatrix}_{(m \times n)}. \quad (10)$$

Finally, the vector of coefficients for the RBFs is

$$\mathbf{a}^T = \{a_1 \ a_2 \ \dots \ a_n\}, \quad (11)$$

and the vector of coefficients for the polynomial is given by

$$\mathbf{b}^T = \{b_1 \ b_2 \ \dots \ b_n\}. \quad (12)$$

In Eq. 9, the distance r_k occurring in $R_i(r_k)$ is obtained by

$$r_k = \sqrt{(x_k - x_i)^2 + (y_k - y_i)^2}. \quad (13)$$

At this point it should be noted, that there are $n + m$ variables in Eq. 7. The additional m equations can be added using the following m constraint conditions

$$\sum_{i=1}^n p_j(\mathbf{x}_i) a_i = \mathbf{P}_m^T \mathbf{a} = 0, \quad j = 1, 2, \dots, m. \quad (14)$$

Combining Eq. 7 and Eq. 14 yields a set of equations, here given in matrix notation, such that

$$\tilde{\mathbf{U}}_s = \begin{bmatrix} \mathbf{U}_s \\ \mathbf{0} \end{bmatrix} = \underbrace{\begin{bmatrix} \mathbf{R}_0 & \mathbf{P}_m \\ \mathbf{P}_m^T & \mathbf{0} \end{bmatrix}}_{\mathbf{G}} \begin{Bmatrix} \mathbf{a} \\ \mathbf{b} \end{Bmatrix} = \mathbf{G}\mathbf{a}_0, \quad (15)$$

where

$$\mathbf{a}_0^T = \{\mathbf{a}_1 \ \mathbf{a}_2 \ \cdots \ \mathbf{a}_n \ \mathbf{b}_1 \ \mathbf{b}_2 \ \cdots \ \mathbf{b}_m\}, \quad (16)$$

$$\tilde{\mathbf{U}}_s = \{\mathbf{u}_1 \ \mathbf{u}_2 \ \cdots \ \mathbf{u}_n \ \mathbf{0} \ \mathbf{0} \ \cdots \ \mathbf{0}\}. \quad (17)$$

Since the matrix \mathbf{R}_0 is symmetric, the matrix \mathbf{G} will also be symmetric.

Solving Eq. 15 yields

$$\mathbf{a}_0 = \begin{Bmatrix} \mathbf{a} \\ \mathbf{b} \end{Bmatrix} = \mathbf{G}^{-1}\tilde{\mathbf{U}}_s. \quad (18)$$

Re-writing Eq. 5, such that

$$u(\mathbf{x}) = \mathbf{R}^T(\mathbf{x})\mathbf{a} + \mathbf{p}^T(\mathbf{x})\mathbf{b} = \{ \mathbf{R}^T(\mathbf{x}) \ \mathbf{p}^T(\mathbf{x}) \} \begin{Bmatrix} \mathbf{a} \\ \mathbf{b} \end{Bmatrix}, \quad (19)$$

and using Eq. 18, one obtains

$$u(\mathbf{x}) = \{ \mathbf{R}^T(\mathbf{x}) \ \mathbf{p}^T(\mathbf{x}) \} \mathbf{G}^{-1}\tilde{\mathbf{U}}_s = \tilde{\Phi}^T(\mathbf{x})\tilde{\mathbf{U}}_s, \quad (20)$$

where the RPIM shape functions can be expressed as

$$\begin{aligned} \tilde{\Phi}^T(\mathbf{x}) &= \{ \mathbf{R}^T(\mathbf{x}) \ \mathbf{p}^T(\mathbf{x}) \} \mathbf{G}^{-1} \\ &= \{ \phi_1(\mathbf{x}) \ \phi_2(\mathbf{x}) \ \cdots \ \phi_n(\mathbf{x}) \ \phi_{n+1}(\mathbf{x}) \ \cdots \ \phi_{n+m}(\mathbf{x}) \} \end{aligned} \quad (21)$$

Finally, the according shape functions corresponding to the nodal displacements vector $\Phi(x)$ are obtained as

$$\Phi^T(\mathbf{x}) = \{ \phi_1(\mathbf{x}) \ \phi_2(\mathbf{x}) \ \cdots \ \phi_n(\mathbf{x}) \}, \quad (22)$$

Eq. 20 can be re-written such that

$$u(\mathbf{x}) = \Phi^T(\mathbf{x})\mathbf{U}_s = \sum_{i=1}^n \phi_i u_i, \quad (23)$$

and the derivatives of $u(\mathbf{x})$ are easily obtained as

$$u_{,l}(\mathbf{x}) = \Phi_{,l}^T(\mathbf{x})\mathbf{U}_s, \quad (24)$$

where l denotes either the coordinates x or y . A comma designates a partial differentiation with respect to the indicated spatial coordinate that follows.

RPIM shape functions have the kronecker delta function property, that is

$$\phi_i(\mathbf{x}_j) = \delta_{ij} = \begin{cases} 1 & i = j \\ 0 & i \neq j \end{cases}. \quad (25)$$

This is because the RPIM shape functions are created to pass through nodal values. They also have the property of partitions of unity, i.e.

$$\sum_{i=1}^n \phi_i(\mathbf{x}) = 1, \quad (26)$$

when the linear polynomial terms are added in the basis, and hence there is a constant term in the basis functions. This is a necessary condition for the shape function to be able to produce any rigid body motion of the problem domain. These added polynomials also ensure an exact reproduction of linear polynomials.

RPIM shape functions are compactly supported, as they are constructed using nodes in a compact support domain, and they are not used or regarded as zero outside the support domain. They also possess higher continuity because of the high continuity of the radial basis functions.

However, in using RPIM shape functions, the compatibility in the global domain is not ensured when the local support domain is used, and the field function approximated could be discontinuous when nodes enter or leave the moving support domain. The nodes in the support domain are updated suddenly, meaning that when the nodes are entering or leaving the support domain, they are actually jumping into or out of the support domain [Liu and Gu (2005)]. Care must be taken when a global weak-form is used together with RPIM shape functions with compact supports. A parameter assessment has been performed by the authors to determine the optimum RPIM parameters that render accurate and continuous results for composites [Djeukou and von Estorff (2009)].

3 Third order shear deformation theory

As a representative shear deformable laminate, a laminate plate of $a \times b \times c$ as shown in Fig. 3 is considered. The displacements of the plate in the (x, y, z) directions are denoted as (u, v, w) , respectively. Based on the third order deformation theory given by Reddy [Reddy (1997)], the displacement field within one layer is

assumed to be

$$\begin{Bmatrix} u \\ v \\ w \end{Bmatrix} = \begin{bmatrix} 1 & 0 & -\gamma z^3 \frac{\partial}{\partial x} & z - \gamma z^3 & 0 \\ 0 & 1 & -\gamma z^3 \frac{\partial}{\partial y} & 0 & z - \gamma z^3 \\ 0 & 0 & 1 & 0 & 0 \end{bmatrix} \begin{Bmatrix} u_0 \\ v_0 \\ w_0 \\ \phi_x \\ \phi_y \end{Bmatrix} \text{ or } \mathbf{u} = \mathbf{H}\mathbf{u}_0, \quad (27)$$

where $\gamma = 4/(3h^2)$, h is the thickness of the laminate, and (u_0, v_0, w_0) are the displacements of a point on the neutral-plane in the (x, y, z) direction, respectively.

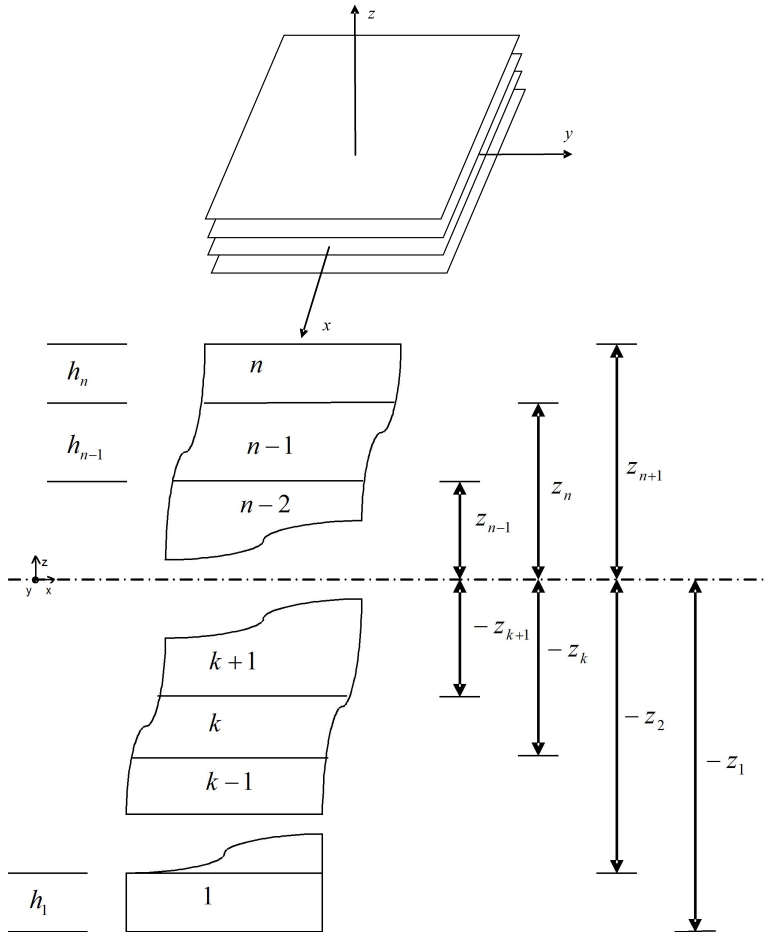


Figure 3: A typical laminate plate and its coordinate system

(ϕ_x, ϕ_y) are the rotations about the (x, y) axis. They are defined as

$$\mathbf{u}_0 = \begin{Bmatrix} u_0 \\ v_0 \\ w_0 \\ \phi_x \\ \phi_y \end{Bmatrix} = \sum_{I=1}^n \begin{bmatrix} \phi_{uI} & 0 & 0 & 0 & 0 \\ 0 & \phi_{vI} & 0 & 0 & 0 \\ 0 & 0 & \phi_{wI} & 0 & 0 \\ 0 & 0 & 0 & \phi_{xI} & 0 \\ 0 & 0 & 0 & 0 & \phi_{yI} \end{bmatrix} \begin{Bmatrix} u_I \\ v_I \\ w_I \\ \phi_{xI} \\ \phi_{yI} \end{Bmatrix} = \sum_{I=1}^n \Phi_I \mathbf{u}_I, \quad (28)$$

where n is the number of nodes in the support domain of a point of interest x and $\phi_{uI}, \phi_{vI}, \phi_{wI}, \phi_{xI}, \phi_{yI}$ are different shape functions which may be independent of each other. It should be noted, that in this work, the shape functions in all directions are set to be equal. The linear strains are given by

$$\begin{Bmatrix} \varepsilon_{xx} \\ \varepsilon_{yy} \\ \varepsilon_{xy} \\ \varepsilon_{xz} \\ \varepsilon_{yz} \end{Bmatrix} = \begin{bmatrix} \frac{\partial}{\partial x} & 0 & -\gamma z^3 \frac{\partial^2}{\partial x^2} & (z - \gamma z^3) \frac{\partial}{\partial x} & 0 \\ 0 & \frac{\partial}{\partial y} & -\gamma z^3 \frac{\partial^2}{\partial y^2} & 0 & (z - \gamma z^3) \frac{\partial}{\partial y} \\ \frac{\partial}{\partial y} & \frac{\partial}{\partial x} & -2\gamma z^3 \frac{\partial^2}{\partial x \partial y} & (z - \gamma z^3) \frac{\partial}{\partial y} & (z - \gamma z^3) \frac{\partial}{\partial x} \\ 0 & 0 & (1 - \beta z^2) \frac{\partial}{\partial x} & (1 - \beta z^2) & 0 \\ 0 & 0 & (1 - \beta z^2) \frac{\partial}{\partial y} & 0 & (1 - \beta z^2) \end{bmatrix} \begin{Bmatrix} u_0 \\ v_0 \\ w_0 \\ \phi_x \\ \phi_y \end{Bmatrix}$$

or

$$\boldsymbol{\varepsilon}_p = \mathbf{L} \mathbf{u}_0, \quad (29)$$

where $\beta = 3\gamma$.

Since most laminates are typically rather thin, a plane state of stress may be assumed. For an orthotropic laminate ply, the strain-stress relations can be written in the ply local coordinate system in the form to obtain

$$\boldsymbol{\sigma}_p = \mathbf{D} \boldsymbol{\varepsilon}_p, \quad \mathbf{D} = \begin{bmatrix} Q_{11} & Q_{12} & 0 & 0 & 0 \\ Q_{12} & Q_{22} & 0 & 0 & 0 \\ 0 & 0 & Q_{66} & 0 & 0 \\ 0 & 0 & 0 & Q_{44} & 0 \\ 0 & 0 & 0 & 0 & Q_{55} \end{bmatrix}. \quad (30)$$

The different Q_{ij} values are given by

$$Q_{11} = \frac{E_1}{1 - \nu_{12}\nu_{21}}, \quad Q_{12} = \frac{\nu_{12}E_2}{1 - \nu_{12}\nu_{21}}, \quad Q_{22} = \frac{E_2}{1 - \nu_{12}\nu_{21}},$$

$$Q_{66} = G_{12}, \quad Q_{44} = G_{13}, \quad Q_{55} = G_{23}, \quad \nu_{21}E_1 = \nu_{12}E_2 \quad (31)$$

in which (E_i, G_{ij}, ν_{ij}) are Young's modulus, the shear modulus, and Poisson's ratio, respectively. The subscript 1 denotes the principle material (or fibre) direction.

For analysis purposes, the material matrices of all plies of the laminate shall be transformed in the laminate global coordinate systems as follows:

$$\bar{\sigma}_p = \bar{\mathbf{D}}\bar{\epsilon}_p, \bar{\mathbf{D}} = \mathbf{T}_\sigma \mathbf{D} \mathbf{T}_\epsilon^{-1}, \quad (32)$$

where \mathbf{T}_σ and \mathbf{T}_ϵ are the stresses and strains transformation matrix respectively. They are defined as

$$\mathbf{T}_\sigma = \begin{bmatrix} \cos^2(\alpha) & \sin^2(\alpha) & 2\sin(\alpha)\cos(\alpha) & 0 & 0 \\ \sin^2(\alpha) & \cos^2(\alpha) & -2\sin(\alpha)\cos(\alpha) & 0 & 0 \\ -\sin(\alpha)\cos(\alpha) & \sin(\alpha)\cos(\alpha) & \cos^2(\alpha) - \sin^2(\alpha) & 0 & 0 \\ 0 & 0 & 0 & -\cos(\alpha) & -\sin(\alpha) \\ 0 & 0 & 0 & \sin(\alpha) & -\cos(\alpha) \end{bmatrix}, \quad (33)$$

$$\mathbf{T}_\epsilon = \begin{bmatrix} \cos^2(\alpha) & \sin^2(\alpha) & \sin(\alpha)\cos(\alpha) & 0 & 0 \\ \sin^2(\alpha) & \cos^2(\alpha) & -\sin(\alpha)\cos(\alpha) & 0 & 0 \\ -2\sin(\alpha)\cos(\alpha) & 2\sin(\alpha)\cos(\alpha) & \cos^2(\alpha) - \sin^2(\alpha) & 0 & 0 \\ 0 & 0 & 0 & -\cos(\alpha) & -\sin(\alpha) \\ 0 & 0 & 0 & \sin(\alpha) & -\cos(\alpha) \end{bmatrix}, \quad (34)$$

where α is the angle of the fibre orientation of the ply, i.e., the ply angle.

4 Modeling of damage in composites

A two-dimensional Tsai-Wu failure criterion is used to predict a layer failure in the laminate. In Tsai-Wu general quadratic interaction criteria [Tsai and Wu (1971)], the failure surface in stress space is described as

$$F_1\sigma_x + F_2\sigma_y + F_{11}\sigma_x^2 + F_{22}\sigma_y^2 + F_{44}\tau_{yz}^2 + F_{55}\tau_{xz}^2 + F_{66}\tau_{xy}^2 + 2F_{12}\sigma_x\sigma_y \leq 1 \quad (35)$$

where $\sigma_i (i = 1, 2)$ and $\tau_{ij} (i = 1, 2; j = 1, 2, 3)$ are the normal and shear stress components with respect to the material axes. The following strength parameters account for the laminate failure:

$$\begin{aligned}
F_1 &= \frac{1}{\sigma_{xTM}} - \frac{1}{\sigma_{xCM}} & F_2 &= \frac{1}{\sigma_{yTM}} - \frac{1}{\sigma_{yCM}} \\
F_{11} &= \frac{1}{\sigma_{xTM}\sigma_{xCM}} & F_{22} &= \frac{1}{\sigma_{yTM}\sigma_{yCM}} \\
F_{12} &= -\frac{1}{2\sqrt{\sigma_{xTM}\sigma_{xCM}\sigma_{yTM}\sigma_{yCM}}} & F_{44} &= \frac{1}{\tau_{yzM}^2} \\
F_{55} &= \frac{1}{\tau_{xzM}^2} & F_{66} &= \frac{1}{\tau_{12M}^2}
\end{aligned} \tag{36}$$

where σ_{xTM} and σ_{xCM} are the longitudinal tensile and compressive strengths, σ_{yTM} , σ_{yCM} the transverse tensile and compressive strengths, and τ_{xyM} , τ_{yzM} , τ_{xzM} the shear strengths in the x-y, y-z, and x-z plane, respectively.

The result of the left-hand side of Eq. 35 is often called a failure index, since damage is predicted when this index exceeds one at a considered point. The stresses in the failure criteria Eq. 35 are assumed to exist in the material axes, such that the stresses calculated at a node location must be transformed in the direction of these axes. The index will be calculated at every nodes in the discretized domain and at every layers of the laminate to determine whether damage occurred or not.

A weakness of using the Tsai-Wu quadratic failure equation is, that it can predict damage occurrence but it cannot differentiate between damage modes (matrix or fibre failure). Since the impact-induced damage strongly depends on the damage modes, an additional criterion needs to be used in conjunction with the Tsai-Wu failure criteria. The corresponding stiffness term of the stiffness matrix in Eq. 30 will be reduced following the damage mode, and stresses will be updated.

If $\sigma_x \geq 0$ and $\sigma_x \leq \sigma_{xTM}$ or $\sigma_x \leq 0$ and $\sigma_x \geq \sigma_{xCM}$, it is assumed that there is a matrix failure, and the elastic constants E_2 and G_{23} at the failure location are set to zero. Consequently, due to the presence of the matrix damage, the damaged node cannot hold any additional transverse tensile stress and out-of-plane shear stress anymore. On the other hand, if $\sigma_x \geq 0$ and $\sigma_x \geq \sigma_{xTM}$ or $\sigma_x \leq 0$ and $\sigma_x \leq \sigma_{xCM}$, the fibres are considered to be damaged. Then the elastic constants E_1 , E_2 , G_{12} and G_{13} are set to zero at failure location and the damage node can carry no further in-plane load.

Besides of the intra laminate damage modes, a criterion to find delamination of the interface between two kinds of orientation ply groups is incorporated [Zhao and Cho (2004)]:

$$f_d = \left(\frac{\tau_{xz}}{\tau_{xzM}} \right)^2 + \left(\frac{\tau_{yz}}{\tau_{yzM}} \right)^2 \geq 1 \tag{37}$$

If delamination occurs, the corresponding stress components are reduced to zero by setting the elastic constants G_{13} and G_{23} to zero.

Through out the analysis, the following steps will be performed:

- (1) The maximum impact contact force and the according stresses are computed for each node.
- (2) The stresses are transformed to the material axes to calculate the failure index by means of Tsai-Wu criterion.
- (3) If the damage is predicted, the longitudinal stress component σ_1 is first checked to determine whether matrix failure or fibre failure occurs in the lamina. Then it is checked whether delamination occurs between the layers. Finally the appropriate lamina moduli are reduced at the damage location and the stresses are recalculated.

5 Discrete system of equations

The static equations of a laminated plate can be derived by applying the principle of virtual work to an elastic structure under static loading. The principle requires that the work of discrete forces, body forces, and surface tractions due to an infinitesimal virtual displacement should be equal to the sum of strain energy and dissipated strain energy variations, i.e.,

$$\int_{\Omega} \delta \mathbf{u}^T \mathbf{b} d\Omega + \int_{\Gamma_t} \delta \mathbf{u}^T \bar{\mathbf{t}} d\Gamma = \int_{\Omega} \delta \varepsilon^T \sigma d\Omega \quad (38)$$

where $\int_{\Omega} \delta \mathbf{u}^T \mathbf{b} d\Omega$ is the virtual work of non-inertial body forces, and $\int_{\Gamma_t} \delta \mathbf{u}^T \bar{\mathbf{t}} d\Gamma$ is the virtual work of the surface tractions. The term $\int_{\Omega} \delta \varepsilon^T \sigma d\Omega$ denotes the variation of the specific strain energy.

Substituting Eq. 28 into Eq. 38, one obtains

$$\mathbf{K}\mathbf{U} = \mathbf{F}, \quad (39)$$

where the stiffness matrix \mathbf{K} and the force vector \mathbf{F} are formed by assembling the matrices and vectors associated with the nodes I and J , and with the layer k , as given by

$$\mathbf{K} = \sum_{k=1}^P \sum_{I=1}^N \sum_{J=1}^N \mathbf{K}_{kJJ} \quad (40)$$

$$\mathbf{K}_{kJJ} = \int_{\Omega} \int_{z_k}^{z_{k+1}} \Phi_I^T \mathbf{L}^T \mathbf{D} \mathbf{L} \Phi_J dz d\Omega = \int_{\Omega} \int_{z_k}^{z_{k+1}} (\mathbf{B}_I^T)_{5 \times 5} \mathbf{D} (\mathbf{B}_J)_{5 \times 5} dz d\Omega$$

$$\mathbf{F} = \sum_{k=1}^P \sum_{I=1}^N \mathbf{F}_{kI} ; \quad \mathbf{F}_{kI} = \mathbf{F}^b + \mathbf{F}^t = \int_{\Omega} \int_{z_k}^{z_{k+1}} \mathbf{A}_I^T \mathbf{b} dz d\Omega + \int_{\Gamma_t} \int_{z_k}^{z_{k+1}} \mathbf{A}_I^T \bar{\mathbf{t}} dz d\Gamma \quad (41)$$

$$\mathbf{A}_I = \mathbf{H}\Phi_I = \begin{bmatrix} \phi_{uI} & 0 & -\gamma z^3 \phi_{wI,x} & (z - \gamma z^3) \phi_{xI} & 0 \\ 0 & \phi_{vI} & -\gamma z^3 \phi_{wI,y} & 0 & (z - \gamma z^3) \phi_{yI} \\ 0 & 0 & \phi_{wI} & 0 & 0 \end{bmatrix} \quad (42)$$

$$\mathbf{B}_I = \mathbf{L}\Phi_I = \begin{bmatrix} \phi_{uI,x} & 0 & -\gamma z^3 \phi_{wI,xx} & (z - \gamma z^3) \phi_{xI,x} & 0 \\ 0 & \phi_{vI,y} & -\gamma z^3 \phi_{wI,yy} & 0 & (z - \gamma z^3) \phi_{yI,y} \\ \phi_{uI,y} & \phi_{vI,x} & -2\gamma z^3 \phi_{wI,xy} & (z - \gamma z^3) \phi_{xI,y} & (z - \gamma z^3) \phi_{yI,x} \\ 0 & 0 & (1 - \beta z^2) \phi_{wI,x} & (1 - \beta z^2) \phi_{xI} & 0 \\ 0 & 0 & (1 - \beta z^2) \phi_{wI,y} & 0 & (1 - \beta z^2) \phi_{yI} \end{bmatrix} \quad (43)$$

In Eq. 40, P is the number of layers and N the numbers of nodes. In this work, the force vector is assumed to be applied at $z = 0$. The displacement vector \mathbf{U} in Eq. 39 represents the global nodal parameters. The corresponding nodal displacements are obtained by using Eq. 28. Finally, the penalty method is employed for enforcing the essential boundary condition. For further details see [Djeukou and von Estorff (2008)].

6 Numerical examples

6.1 Model verification

To verify the accuracy of the present model, the contact force determined from the spring-mass model is compared with the contact force determined by means of the Choi's dynamic model and test results [Choi and Lim (2004)]. The present model has been fitted with the conditions in the Choi's paper. As material properties and contact characteristic, the values given in [Choi and Lim (2004)] are assumed. The stacking sequence of laminate is $[90/45/90/-45/90]_{2s}$, geometrical size is 10×10 cm. Tab. 2 shows the various boundary conditions and impact conditions from Choi's paper.

The time history of the contact force displayed in Fig. 4 shows excellent agreement with the results in [Choi and Lim (2004)]. Trends and maximum values can be computed very accurately. λ values mentioned in section 2 were used to consider different boundary conditions. In fact it was found that the suggested approach can be used to compute the contact force history in a rather accurate way.

6.2 Damage after impact

After verification and validation of the impact force history, a $100\text{mm} \times 76\text{mm} \times 2.16\text{mm}$ laminated composite plate with a stacking sequence of $[0_3/90_3/0_3/90_3/0_3]$

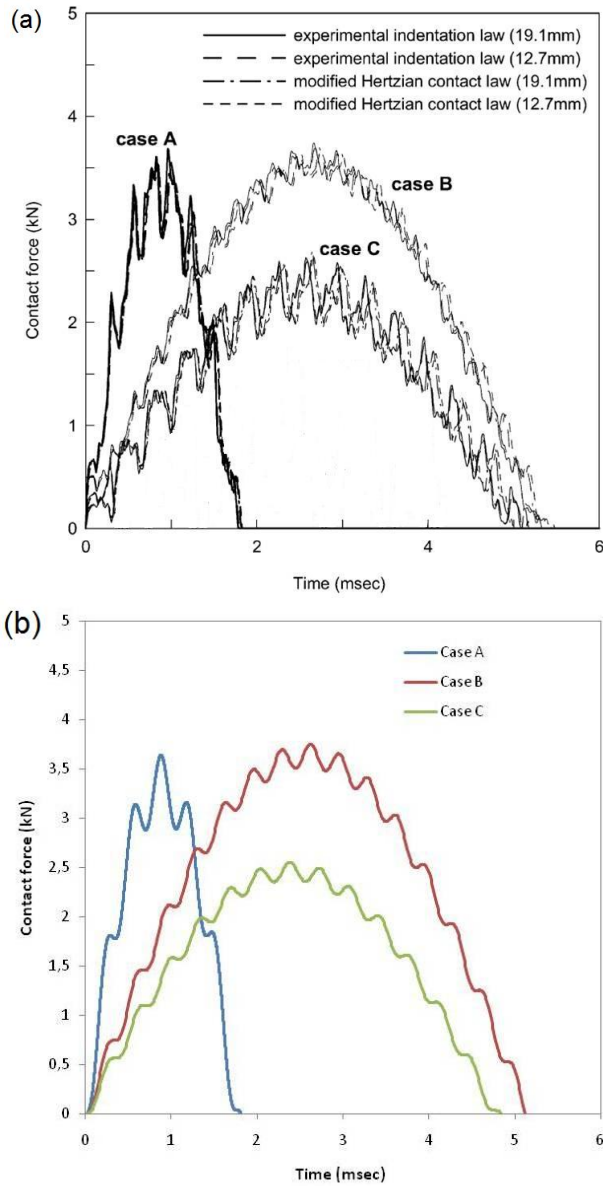


Figure 4: a) Computed and experimental impact force histories from Choi's paper [Choi and Lim (2004)] and b) Computed force histories with the present method

Table 2: Various boundary conditions of laminate and impact conditions of impactor from Choi's paper [Choi and Lim (2004)]

Case ID.	Boundary condition of laminate GPa	Impact condition of impactor	
		M/m^a	Velocity (cm/sec)
A	4 edges fixed	8.75	500.
B	4 edges fixed	80.	175.
C	4 edges simply supported	35.	250.

^a M/m is ratio between masses of impactor and laminate

under impact load was analysed in order to evaluate the impact-induced damage area. The initial impact velocity is 6.7 m/s and the impactor mass 0.16 kg. The plate is clamped along two edges and not supported at the other two. A 17×13 regular node distribution was considered assuming the material property of T300/976 [Zhao and Cho (2004)].

The results are compared to those given by Zhao [Zhao and Cho (2004)] and displayed in Fig. 5. They present the calculated failure indices at an interface between the 0° and 90° layers. Fig. 6 shows the damages measured as described in [Choi and Chang (1992)]. Very good correlations could be reached, pointing out, once more, that the new methodology is able to predict damages in composite plates rather accurately.

6.3 Dent depth

To evaluate the accuracy of a dent depth prediction using the present approach, some examples were analyzed and compared with test results given in [Uyaner and Kara (2007)]. A $180\text{mm} \times 100\text{mm} \times 7\text{mm}$ E-glass/epoxy composite panel consisting of 18-ply with a stacking sequence of $[0/-45/45/0/90/0/45/-45/0]_s$ was impacted by a 3 kg mass with a radius of 12 mm. Three different velocities have been applied: 2.0, 2.5 and 3.0 m/s. Two sides of the panel are clamped and the other two are not supported. The material properties are the same as in [Uyaner and Kara (2007)]. A 11×11 regular node distribution was considered.

Tab. 3 shows the measured dent depth from [Uyaner and Kara (2007)] and the calculated one from the present methods. In case of low velocities, conservative results could be obtained. The conservatism decrease with increasing impact velocity.

7 Conclusions

In this article, the response of rectangular composite plates to low-velocity impact has been studied. A third-order shear deformation theory (TSDT) as well as the

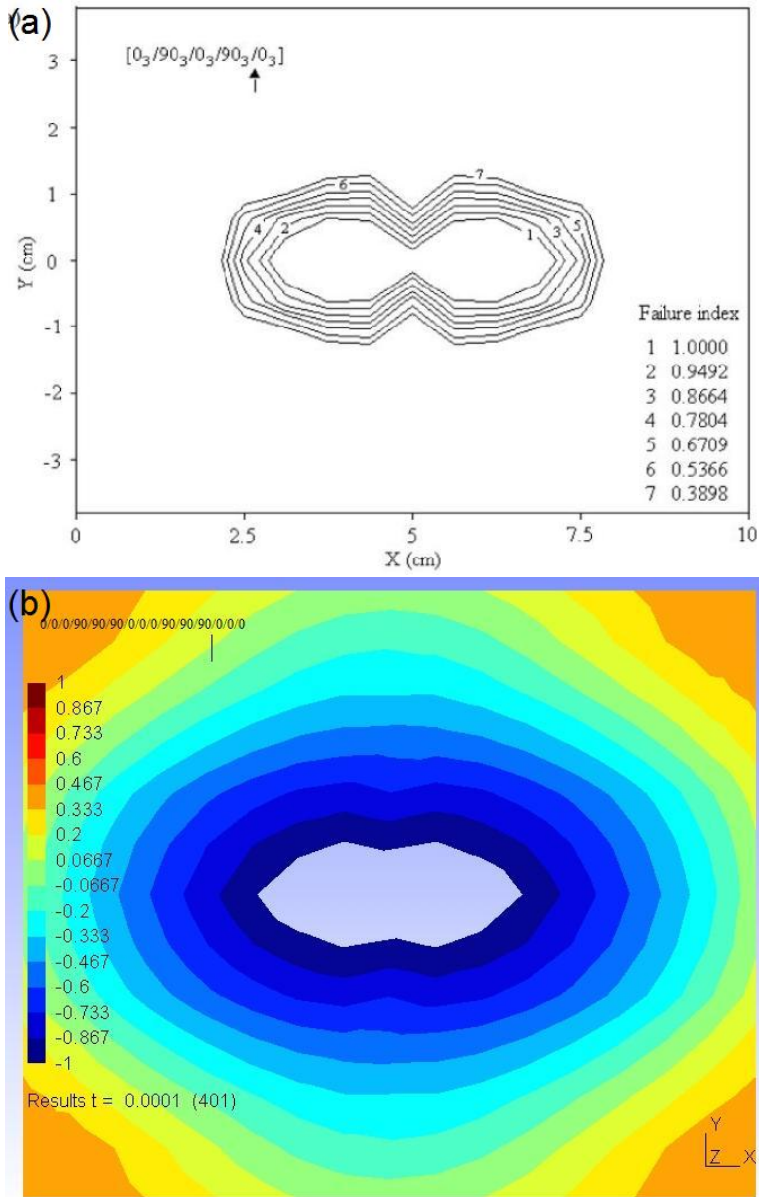


Figure 5: a) Calculated failure index [Zhao and Cho (2004)] and b) Calculated failure index from the present work



Figure 6: Experiment delamination in the plate [Choi and Chang (1992)]

Table 3: Dent depths obtained from the low-velocity impact tests from [Uyaner and Kara (2007)] and from computation with the present method

Velocity (m/s)	Dent (mm) [Uyaner and Kara (2007)]	present method (mm)	Difference
2.0	10.9	13.5	23.8 %
2.5	13.1	14.5	10.7 %
3.0	16.4	15.7	-4.3 %

newmark integration were used to determine the contact force history analytically. The interaction between the impactor and the plate was modeled with the help of two degrees-of-freedom spring-mass model. The Choi's linearized Hertzian contact model was applied to determine the contact force. Then the determined maximum impact force was considered for a static damage analysis of the composite plate using the radial point interpolation method (RPIM). The damage surface resulting from the impact on the composite plate was computed using the Tsai-Wu failure criterion.

Several examples have been investigated to verify and validate the suggested approach. Force history, damage and dent depth were compared to analytical and test results available in the literature. It was found that the suggested approach can be used in a rather accurate way.

References

- Abrate, S.** (2001): Modeling of impacts on composite structures. *Composite structures*, vol. 51, pp. 129–138.
- Cantwell, W. J.; Morton, J.** (1991): The impact resistance of composite materials - a review. *Composites*, vol. 5, pp. 347–362.
- Chen, X. L.; Liu, G. R.; Lim, S. P.** (2003): An element free galerkin method for free vibration analysis of composite laminates of complicated shape. *Composite structures*, vol. 59, pp. 279–289.
- Choi, H. Y.; Chang, F. K.** (1992): A model for predicting damage in graphite/epoxy laminated composites resulting from low-velocity point impact. *Journal of composite materials*, vol. 26, pp. 2134–2169.
- Choi, I. H.; Lim, C. H.** (2004): Low-velocity impact analysis of composite laminates using linearized contact law. *Composite structures*, vol. 66, pp. 125–132.
- Djeukou, A.; von Estorff, O.** (2008): Static and damage analysis of shear deformable laminated composites plates using the radial point interpolation method. *Progress on meshless methods, Series: Computational methods in applied mechanics*, vol. 11, pp. 199–216.
- Djeukou, A.; von Estorff, O.** (2009): Assessment of different rpim parameters for static analyses of shear deformable laminated composite plates. *Computational Mechanics*, vol. 44/3, pp. 423–431.
- Hagihara, S.; Tsunori, M.; Ikeda, T.; Miyazaki, N.** (2007): Application of meshfree method to elastic-plastic fracture mechanics parameter analysis. *CMES: Computer Modeling in Engineering & Sciences*, vol. 17/2, pp. 63–72.
- Jarak, T.; Sori, J.; Hoster, J.** (2007): Analysis of shell deformation responses by the meshless local petrov-galerkin (mlpg) approach. *CMES: Computer Modeling in Engineering & Sciences*, vol. 18/3, pp. 235–246.
- Khalili, S. M. R.; Shokuhfar, A.; Ashenai Ghasemi, F.** (2007): Dynamic response of smart hybrid composite plate subjected to low-velocity impact. *Journal of composite materials*, vol. 41, pp. 2347–2370.
- Krysl, P.; Belytschko, T.** (1995): Analysis of thin plates by the element-free galerkin method. *Computational mechanics*, vol. 17, pp. 26–35.

Liu, G. R. (2002): *Mesh free methods: moving beyond the finite element method*. New-york, crc press edition.

Liu, G. R.; Gu, Y. T. (2001): A local radial point interpolation method (lr-rpim) for free vibration analysis of 2-d solids. *Journal of sound and vibration*, vol. 246, pp. 29–46.

Liu, G. R.; Gu, Y. T. (2005): *An introduction to meshfree methods and their programming*. Springer edition.

Reddy, J. N. (1997): *Mechanics of laminated composite plates - theory and analysis*. New-york, crc press edition.

Shan, Y.; Shu, C.; Lu, Z. (2008): Application of local mq-dq method to solve 3d incompressible viscous flows with curved boundary. *CMES: Computer Modeling in Engineering & Sciences*, vol. 25/2, pp. 99–114.

Sladek, J.; Sladek, V.; Zhang, C.; Solek, P.; Starek, L. (2007): Fracture analyses in continuously nonhomogeneous piezoelectric solids by the mlpg. *CMES: Computer Modeling in Engineering & Sciences*, vol. 19/3, pp. 247–262.

Sun, C. T. (1977): An analytical method for evaluation of impact damage energy of laminated composites. *Am. Soc. Test. Mater., ASTM STP*, vol. 617, pp. 427–440.

Tsai, S. W.; Wu, E. M. (1971): A general theory of strength for anisotropic materials. *Journal of Composite Materials*, vol. 5/1, pp. 58–80.

Uyaner, M.; Kara, M. (2007): Dynamic response of laminated composites subjected to low-velocity impact. *Journal of composite materials*, vol. 41, pp. 2877–2896.

Wen-Hwa, C.; Cheng-Te, C.; Ming-Hsiao, L. (2009): A novel element-free galerkin method with uniform background grid for extremely deformed problems. *CMES: Computer Modeling in Engineering & Sciences*, vol. 40/2, pp. 175–200.

Willis, J. R. (1966): Hertzian contact of anisotropic bodies. *J Mech Phys Solids*, vol. 14, pp. 163–176.

Yang, S. H.; Sun, C. T. (1981): Indentation law for composite laminates. *Am. Soc. Test. Mater., ASTM STP*, vol. 787, pp. 425–449.

Zhao, G.; Cho, C. (2004): On impact damage of composite shells by low-velocity projectile. *Journal of composite materials*, vol. 38, pp. 1231–1254.